IRRADIATION AND ANNEALING BEHAVIOUR OF HEAVY ION IMPLANTED SILICON BY TEM AND THE CHANNELING-BACKSCATTERING TECHNIQUE

by

HAROLD K. HAUGEN, B.Sc. (PHYSICS)

PART B: McMASTER (ON-CAMPUS) PROJECT*

A Report
Submitted to the School of Graduate Studies
in Partial Fulfilment of the Requirements
for the degree

Master of Engineering

Department of Engineering Physics
McMaster University
Hamilton, Ontario, Canada

December 1978

*One of two Project Reports: The other part is designated
PART A: OFF-CAMPUS PROJECT

MASTER OF ENGINEERING (1978) McMASTER UNIVERSITY
Department of Engineering Physics Hamilton, Ontario

TITLE: Irradiation and Annealing Behaviour of Heavy Ion Implanted Silicon by TEM and the Channeling Backscattering Technique

AUTHOR: Harold K. Haugen, B.Sc. (Acadia)

SUPERVISOR: Dr. D.A. Thompson

NUMBER OF PAGES: vi, 51

ACKNOWLEDGEMENTS

I wish to thank my supervisor, Dr. D.A. Thompson and Larry Howe[a], for their direction of this research.

Thanks are also extended to Dr. J.A. Davies[b] for interesting discussions during the course of this work.

(a),(b) Solid State Science Branch, Atomic Energy of Canada, Chalk River, Ontario.

ABSTRACT

Recent channeling-backscattering measurements of the disorder induced by heavy ion irradiation of semiconductors has indicated radiation damage far in excess of that predicted by linear transport theory. The present work extends the investigation to TEM and compares the two techniques in an annealing study of ion irradiated silicon ($\sim$ 80-200 a.m.u. ions of 15-100 keV) for low fluence (typically $3\times10^{11}/cm^2$ for TEM and 10^{12}-$10^{13}/cm^2$ for channeling) bombardment. In addition to showing a good correlation between the techniques, the results indicate that neither does there exist a unique relationship between lattice disordering and cascade energy density, nor that a well defined amorphous structure seems to exist.

TABLE OF CONTENTS

TABLES AND FIGURES

CHAPTER I

INTRODUCTION

Channeling-backscattering measurements of ion implantation in silicon show significant deviations from the predictions of linear transport theory - the discrepency generally increasing with ion mass. Such results support an "energy spike" model, predicting damage enhancement resulting from localized melting of the lattice.

Although several electron microscopy studies of ion irradiated silicon have been performed, investigations typically involved highly disordered surface layers or regimes with significant cascade overlap. This study compares the two techniques in investigations of heavy ion irradiated silicon, where TEM reveals isolated cascades, and channeling, deviations from a binary collision model.

Solid state disorder represents the result of competing displacement and annealing processes. In order to further investigate the role of energy density and diatomic irradiation effects on the structure of the cascade volume, correlated studies of annealing behaviour were performed for three ion species (As^+, Bi^+, Sb_2^+).

Although ion implantation technology for semiconductor devices has prompted much interest in ion-induced radiation damage, such studies also serve to give more insight into basic physical mechanisms of lattice disordering which elude description by equilibrium physics.

CHAPTER II

THEORY

2.1 The Stopping Cross Section

The interaction between an energetic charged particle and a target atom is typically described by a cross section. Hence probability concepts lie at the foundations of measurement processes in atomic collisions. It is thus impossible to predict "a priori" the exact nature of the interaction of the individual ion with the target. However, since a large number of particles are involved in any single measurement, an average is obtained whose precision can be estimated with Poisson statistics.

The interaction of a charged particle with a solid is in general complex, depending on projectile, target and energy regime. The quantity of interest is the stopping power of the target defined by:

$$\frac{dE}{dx}(E) = \lim_{\Delta x \to o} \frac{\Delta E}{\Delta x} \tag{1}$$

From a microscopic point of view the expectation value of the energy loss may be described in terms of the probabilities, P_i, for various interactions. With N, the number density of target atoms, the stopping power becomes:

$$\frac{\langle \Delta E \rangle}{\Delta x} = \sum_i T_i P_i = N \int T \, d\sigma$$

where T_i is a particular energy transfer to a target atom and, $d\sigma$, the continuum analog of P_i - the differential scattering probability. The integral above is termed the stopping cross section, S(E), which is in general a more useful quantity than the stopping power, because of the normalization to a single atom.

2.2 Inelastic Energy Loss

Charged particles with energies typical of ion implantation interact with a solid primarily by excitation of target electrons and by Coulomb collisions with target nuclei. Although the electronic and nuclear energy losses are correlated, it is usually a satisfactory approximation to separate their contributions.

For electronic energy loss, classical or semi-classical calculations are feasible in the velocity region where the projectile moves more slowly than the electrons. This region has been treated in detail by Lindhard[1] and Firsov[2]. The quantum theory of stopping applies to high velocity ions and has been well summarized by Bethe[3], Fano[4] and Inokuti[5].

2.3 Nuclear Energy Loss

Whereas a universal electronic stopping power does not exist, Lindhard[6] has developed a universal nuclear stopping curve in terms of a set of reduced parameters.

When the scattering problem is solved by perturbation theory, valid for small θ, and the result is extrapolated to large θ; the differential scattering cross section,

$$d\sigma_n = \pi a^2 \, (dt/2t^{3/2}) \, f(t^{1/2}) \tag{2}$$

is obtained.

Here, t is a reduced energy transfer, and $f(t^{1/2})$ is the universal screening function indicated in Figure 1(a).

The screening function, the reduced energy parameter, ε, and the reduced range parameter ρ may be used to define a universal nuclear stopping cross section, given by:

$$\left(\frac{dE}{d\rho}\right)_n = -S_n(\varepsilon) = \frac{1}{\varepsilon} \int_0^{\varepsilon} f(t^{1/2}) \, d(t^{1/2}) \tag{3}$$

and illustrated in Figure 1(b). The dashed curves represent Lindhard's low velocity approximation to electronic stopping for two ion-solid combinations.

2.4 Radiation Damage and Analysis Techniques

Direct momentum transfer (via nuclear Coulomb collisions) to target atoms of sufficient magnitude for displacement from lattice sites, is the primary mechanism of radiation damage. Such problems have recently received considerable attention because of the significance for nuclear fission, fusion, ion implantation and materials analysis. Summaries of the basic considerations of radiation damage in metals[7] and semiconductors[8] can be found elsewhere.

Several techniques have been developed to investigate radiation induced disorder in a crystalline lattice. The two techniques employed in the present study and yielding quite different information on the disordered solid state are outlined below.

2.4.1 The Channeling-Backscattering Technique

Certain relative orientations of a crystalline lattice and an energetic charged particle result in the gentle steering of the ion by the atomic rows in the lattice - the effect is known as "channeling". Although it was initially of interest for its own right, it has been applied extensively as an analysis technique, including measurement of radiation damage.

Figure 2 shows a schematic of possible ion trajectories in a crystalline solid. Typically, the channeled fraction of the beam accounts for ~98% but this depends on various parameters, including the screening radius and the target temperature. Also indicated is the backscattering yield as a function of the tilt angle of the incident beam with respect to perfect alignment. The channeled particle, A, is prevented from suffering wide angle collisions so that the yield for best alignment results from the small component of the beam which interacts closely with atoms of the first few atomic planes. Between the channeled and random conditions is trajectory B, which "sees" an average atomic density greater than that of a random trajectory.

To supplement this much simplified picture of channeling the reader is referred to the reviews of Gemmel[9] and Morgan[10].

Whereas the channeling effect and the corresponding sensitivity to lattice position relies on nuclear Coulomb collisions, the depth-energy spectrometry of backscattering analysis results from inelastic energy loss. The general features are indicated in Figure 3, with a typical thick target spectrum shown in the lower right hand corner. The energy of a particle scattered from a depth t is given by:

$$E(t) = K^2 \left(E_o - \int_o^t NS(E)\, dt\right) - \int_{t/\cos\phi}^{o} N\, S(E_1)\, dt \qquad (4)$$

where K^2 is the kinematic factor of the collision, N is the atomic density, and S(E) the stopping cross section.

Backscattering yields of MeV light ions used for materials analysis are essentially described by the differential scattering cross section given by Rutherford. The number of atoms per square centimeter of an element in the target may be determined from the Rutherford relation, and the product of the detector solid angle and detector efficiency. Details of the determination of the number of displaced atoms from channeling - backscattering analysis has been presented elsewhere[11].

2.4.2 Transmission Electron Microscopy

Whereas the channeling phenomenon is essentially a problem of classical physics, TEM is a manifestation of the wave nature of the electron. Imaging a specimen with an electron beam can indicate deviation from a perfect crystalline state. If the direct beam is used a so-called bright field image is obtained, whereas the diffracted beam gives the dark field image. For the localized highly disordered regions (in a covalently bonded lattice) of interest to this work it may be assumed that the observed contrast corresponds approximately to the boundary between good crystal and a highly disordered lattice. Directional effects are in this case insignificant.

Since numerous treatments of electron diffraction theory[12] and electron microscopy[13] exist, the details will not be repeated here.

CHAPTER III

EXPERIMENTAL TECHNIQUE

3.1 Introduction

Several experimental techniques have been developed to investigate radiation damage in solids. The techniques discussed earlier, channeling and electron microscopy, can be used to investigate totally different aspects of the disorder. Channeling-backscattering gives the total number of atoms displaced from their lattice sites, but nothing on the nature of the defects. TEM cannot detect isolated defects but gives information on extended defects such as dislocations, stacking faults and amorphous or highly disordered regions.

This study makes quantitative comparisons of the results from the channeling-backscattering technique and TEM. The nature of the measurements necessitated ion fluences for the channeling-backscattering technique which were typically an order of magnitude greater than those used for TEM.

3.2 Damage Measurements by MeV Ion Scattering

Ion implantation and channeling-backscattering analysis were carried out in-situ at the McMaster Tandem Accelerator Laboratory with an on line 3 MeV Van de Graaff accelerator and a 10-150 KeV ion implantation device. Cryogenic cooling of the target allowed implantation to be performed at 50 K. Backscattering analysis was performed by 150°

backscattering of 1 MeV ^{4}He to a silicon surface barrier detector. The ^{4}He beam was collimated with 0.75 mm diameter apertures leading to a half angular divergence of 0.04° - much less than the critical angle for channeling.

For implantation, 2 mm collimating apertures were used with two pairs of electrostatic beam sweep plates, providing rastering of the beam and hence implantation uniformity ($\lesssim$ 5 %) over a 0.42 cm^2 area. Typical implantation current densities were 1-10 na/cm^2. The base pressure in the target chamber was $\lesssim 10^{-6}$ torr but the cryogenic cooling of the inner shield surrounding the target ensures an "effective pressure" of $\lesssim 10^{-10}$ torr at the target surface.

Single crystal silicon of <111> orientation was used in radiation damage measurements. Immediately before mounting in the target chamber the silicon samples were cleaned in a dilute ($\sim$ 10%) HF solution to remove the surface oxide layer. Between the HF treatment and subsequent implantation, the formation of a thin ($\sim$ 1-2 nm in thickness) oxide layer is expected.

Annealing studies by MeV ion backscattering were performed in Chalk River with a 2.5 MeV Van de Graaff. The target chamber and sample preparation was similar to that described above. Annealing was performed in-situ via a small ohmic heater in the goniometer head, coupled to an ac-heater through an isolation transformer. This ensured good current integration by greatly decreasing electrical leakage problems. The ac-heater allowed the target temperature to be raised quickly to the anneal temperature ($\sim$ 1-2 minutes). The temperature was maintained constant for ten minutes (within a couple of degrees Celsius) after

which contact of a grounded copper braid caused the temperature to drop quickly.

Unirradiated spectra, representing a reference for subsequent annealing measurements, were taken as a function of temperature. The target-detector geometry was maintained fixed to ensure the validity of this comparison. To avoid possible annealing effects during backscattering measurements, the target was allowed to cool to $\sim$ 70°C for each analysis. Also the change in temperature over the analysis time is small, allowing a more accurate comparison with the reference curve.

A Nuclear Data ND4420 and ADC were used to collect and display the backscattering spectrum.

3.3 Electron Microscopy

Samples for TEM studies at Chalk River were prepared at the McMaster Tandem Accelerator Laboratory. Sample preparation and typical implantation conditions were described in the previous section. Specimens subsequently analysed by TEM had undergone annealing at room temperature over a period ranging from a few weeks to several months. Comparisons in this study however, are between samples which have annealed for a similar time period.

TEM specimens were prepared from each original irradiated sample by cutting the crystal into four $\sim$(2 mm x 2mm) squares. A specimen was then etched from the unirradiated side by an acid jet (90% conc. HNO_3, 10% HF reagent) until a small hole appeared on the polished irradiated face. Cutting and thinning were performed by mounting the sample in parrafin wax which was later removed by washing in boiling benzene.

This imposes a limitation on the definition of the anneal temperature, since benzene boils at 80°C.

The electron microscope was operated at 100 KeV with a magnification of 1.2×10^5. Typically three areas of the specimen were imaged in both bright and dark field conditions (with $+g = 2\bar{2}0$). Since the print magnification was a factor of two, the final magnification in all cases was 2.4×10^5.

Size distributions of the disordered regions on the print were measured with a travelling microscope. The diameter of a disordered zone represents an average of the maximum and minimum linear dimension. No correlation of closely spaced cascades was taken into account - each being considered separate.

Annealing of specimens was performed at pressures $\sim 10^{-7}$ torr in an electrically heated furnace with an adjustable temperature controller. The temperature was increased to the desired value in $\sim$ 5-10 minutes and the annealing terminated by quickly withdrawing the sample from the chamber using a magnet. No degradation of quality due to oxidation or contamination as a result of repeated annealing was detected.

CHAPTER IV

RESULTS

4.1 Collision Cascade Distribution for Heavy Ion Bombardment of Silicon

Measurements of the distribution of cascade sizes for the following ions were measured by TEM: 60 KeV Bi, 15 KeV Bi, 60 KeV Bi_2, 20 KeV Sb, 40 KeV Sb_2, and 20 KeV As. The original irradiations were performed at 50 K, and TEM measurements carried out at 300 K after long term annealing (several months) at room temperature.

Typically a few hundred disordered regions were measured to establish each of the distributions in Figure 4(a)-(f). A continuous dashed curve has been shown superimposed on the histogram to illustrate the general features. The distributions are normalized to the size interval of maximum occurence. The average diameter indicates an average taken over the maximum and minimum linear dimensions of the disordered region.

Table I summarizes the relevant data for the investigation of ion-irradiated silicon by TEM. Average number densities are indicated, resulting from analyses on three regions on each specimen with expected precision $\sim$ 10%. The average diameter results from several hundred measurements so that relative sizes are expected to have an associated accuracy of a couple of percent.

All irradiations for TEM analysis were performed at a fluence of $3 \times 10^{11}/cm^2$ except for 20 KeV as where $1.05 \times 10^{12}/cm^2$ was used. It should be pointed out that in the case of very heavy ion bombardment (e.g. Bi, Bi_2, Sb_2) the observed number density at room temperature was

less than but close to the original fluence at 50 K. Lighter ion bombardment (e.g. Sb, As) showed a decrease in the observed number density; hence the tendency for a one to one correspondence increases with ion mass (at least in a general way). This must be qualified, however, in that subcascade structure may in some cases contribute significantly to the observed number density. This is expected to be most important for lower mass projectiles and at higher energies.

Although the average diameter will in general differ from the most probable value, Table I shows evidence for scaling with projectile mass. This will be treated in detail later. Figure 4 indicates that those monatomic cascades where the average damage depth is $\gtrsim$ 10 nm (60 KeV Bi, 20 KeV Sb, 20 KeV As) the distribution "tails" to the larger diameters. This can be contrasted with the distribution for 15 KeV Bi which is observed to be approximately Gaussian in shape. The 40 KeV Sb_2 distribution is very broad, whereas 60 KeV Bi_2 is again approximately Gaussian. Table 1 indicates a second analysis performed on the 40 KeV Sb_2 specimen seven months after the first. The shift to a larger average diameter as well as a change in distribution shape (compare Figure 4(e) with Figure 7) indicate possible annealing effects and hence the possibility of non-negligible sample history considerations.

4.2 Annealing Measurements by Channeling-Backscattering Technique

Heavy ion irradiations were performed at 50 K at the McMaster Tandem Accelerator Laboratory to $\sim$ 10% disorder level. These samples were later annealed at the Chalk River Laboratory and analysed by the channeling-backscattering technique. Contrary to indications of early

work in this area annealing at room temperature was determined to be significant for these irradiations as measured by the technique.

The disorder level was measured in-situ after the low temperature irradiation and after warming to room temperature ($\sim$ 15 min - 1/2 hr anneal). The disorder levels were found to reduce significantly: $1.56 \times 10^{16}/cm^2 \rightarrow 1.05 \times 10^{16}/cm^2$ for 15 KeV Sb, $1.31 \times 10^{16} \rightarrow 1.01 \times 10^{16}$ for 15 KeV Bi, $1.71 \times 10^{16} \rightarrow 1.02 \times 10^{16}$ for 15 KeV As, and $1.85 \times 10^{16} \rightarrow 1.68 \times 10^{16}$ for 30 keV Sb_2. A definite mass scaling is evident for monatomic irradiations. Three to four months later all three monatomic-irradiated specimens were analysed in Chalk River to have $\sim 5 \rightarrow 8 \times 10^{15}/cm^2$ disorder level, in excess of the typical surface peak of an unirradiated specimen. Specimens which have been cleaned in a dilute HF solution immediately prior to analysis typically have a disorder level $\sim 7 \times 10^{15}/cm^2$. Since samples in the annealing studies were not cleaned prior to the annealing run it was expected that these specimens had an oxide layer exceeding the thickness for the unirradiated samples used for reference. In order to obtain a first approximation for this correction one specimen was cleaned after the annealing run and remeasured. The adjustment was estimated to be $\sim 2 \times 10^{15}/cm^2$.

The large room temperature recovery raised the possibility of important beam annealing effects. A typical analysis represented a dose of 200 $\mu coul/cm^2$ at McMaster and 600 $\mu coul/cm^2$ at Chalk River. However, collection of spectra in 125 $\mu coul/cm^2$ steps for a second specimen irradiated with 15 KeV Bi revealed no significant beam annealing effect. Also low disorder levels used for the studies also became of concern. However, since the disorder level of the second 15 KeV Bi sample was twice that

of the original, but no significant change in annealing characteristics was observed, confidence in the significance of the fractional remaining disorder levels was obtained.

The annealing results are summarized in Table II and illustrated in Figure 5. The annealing characteristics of the monatomic bombardments show a definite mass scaling, with the heavier ion induced disorder annealing at a higher temperature. Both diatomic cascades anneal at much higher temperatures, with the 30 KeV Sb_2 showing a double annealing stage, whereas the 30 KeV Bi_2 annealing seems to coinside with the higher of the diatomic antimony stages.

4.3 Annealing Investigation with TEM

Table III and Figures 6-8 summarize the TEM investigations of the annealing of ion irradiated silicon. The initial ion fluences at 50 K are shown in brackets. A fluence of $3 \times 10^{11}/cm^2$ was found to give well separated disordered regions for the heavier ions, but in the case of As higher fluences were required to give optimum specimens for TEM. In the case of 40 KeV Sb_2 the residual number density at the highest anneal temperature was still 40% of the room temperature value. The change in distribution shape accounts for the more than comparable decrease in disorder. Both the 15 KeV Bi and 20 KeV As irradiated specimens were annealed to a point where the number density was substantially reduced.

Histograms indicate the densities in 1 nm intervals. Due to the subjective nature of the measurements these intervals have been subdivided solely for the purpose of analysis, as will be discussed later. It should be pointed out that no large changes in distribution shape is evident, even when the higher anneal temperatures are reached. This point will be

discussed later in conjunction with the assumed scaling of the disorder with the linear cascade dimension.

CHAPTER V

DISCUSSION AND CONCLUSIONS

5.1 Theoretical Models - Heavy Ion Bombardment

5.1.1 Breakdown of Linear Transport Theory

Recent experimental studies[14] of heavy ion induced disorder using the channeling-backscattering technique have indicated a discrepency with predictions of linear transport theory. One basic assumption of linear transport theory is that ion-atom and atom-atom collisions closely approximate binary encounters in all collisions involved in the dissipation of energy deposited in nuclear collisions. This is expected to be important in heavy ion irradiations where a large number of atoms are set into motion in a limited cascade volume. In fact, by equating the interatomic distance with the mean free path, it can be shown that for $Sb^+ \rightarrow Si$ the incident ion will transfer on average at least 1 eV at every lattice spacing after the ion energy is below 100 KeV. This should be compared with the heat of melting in silicon which corresponds to 0.8 eV/atom.

The concept of binary collisions obviously becomes invalid for a large number of atoms moving with near thermal velocities. One attempt to describe the microscopic physical processes under such non-linear regimes is that of the "energy-spike", which is outlined below.

5.1.2 The "Energy Spike"

It has been proposed[15] that heavy ion induced cascades may be better described by a limited cascade volume in which the majority of atoms

are in motion - an "energy spike".

The "energy spike" represents a somewhat more conservative description than that of a "thermal spike" which implies that a temperature may be associated with the cascade volume. The concept of temperature is of course associated with equilibrium physics and much controversy exists as to the validity of such models for heavy ion induced cascades. The general features of the "thermal spike" have recently been reviewed by Kelly[16] and will not be repeated here.

Sigmund has assumed local equilibrium in his calculations of the spike half-life and predicted that the lifetime must be at least comparable to the time required to generate the cascade to have significant effect on the lattice. For times shorter than this lifetime, the energy is dissipated too rapidly. It is also expected that the spike be dependent on the energy density of the cascade, at least in a general way. The definition of energy density and past experimental work directed to investigations of its significance in radiation damage processes, is the topic of the next section.

5.1.3 High Energy Density Regimes

The energy density is defined by:

$$\overline{\theta}_{\nu} = \int_{V} \frac{\nu(E)\ F(x,y,z)\ dV}{N \int dV} \qquad (5)$$

in eV/atom, where $F(x,y,z)$ is the spatial distribution of energy deposited in nuclear collisions, the 3-dimensional mapping of $\nu(E)$ - (nuclear deposited energy) , and V is the volume defined by the longitudinal and transverse straggling components, $\langle \Delta z^2 \rangle^{1/2}$ and $\langle x^2 \rangle^{1/2}$ respectively. By determining the ratio between the individual and statistical cascade volumes (by

Monte Carlo simulation), V_R, a realistic volume is defined,

$$V = \frac{4\pi}{3} \langle \Delta z^2 \rangle^{1/2} \langle x^2 \rangle V_R$$

By assuming a three dimensional Gaussian distribution the energy density becomes

$$\overline{\theta}_\nu = 0.2 \, \nu(E)/N \cdot V$$

where N is the atomic number density. The exact magnitude of $\overline{\theta}_\nu$ of course depends on the definition of cascade volume but the general features are insensitive to a precise formulation.

Experimental investigations have indicated the strong dependence of residual lattice disorder on the cascade energy density. One convenient means of varying the energy density is through polyatomic bombardment, since upon impact the molecule splits approximately into atoms of equal energy. The degree of overlap of the atomic cascades depends on the mass ratio (projectile to substrate), with the overlap increasing with the ratio. J.A. Davies[17] et al. found that the damage of polyatomic carbon ion bombardment of silicon at room temperature scaled approximately as n^2, where n is the number of atoms/ion. This work was extended by Thompson and Walker[14] to low temperature irradiations over a wide range of Z_1 (projectile atomic number) on silicon and germanium. Two aspects of the work should be pointed out. The diatomic enhancement is less than that observed for room temperature bombardment, consistent with the qualitative picture of the increased thermal stability of cascades of higher energy density. The enhancement also depends on the mass of the atomic projectile as well as the energy, scaling directly with mass and inversely with energy. Both effects are related to the over-

lap of individual cascades.

The present study involves a correlation of channeling and TEM investigations of heavy ion damage in silicon - cases which involve highly non-linear cascades and in which the "energy spike" concept provides a useful picture of the microscopic processes. The value and possible limitations of the model will be pointed out in conjunction with recent experimental results, but first previous channeling and TEM studies will be discussed.

5.2 Experimental Evidence

5.2.1 Channeling-Backscattering Measurements of Heavy Ion Damage

Irradiations performed to $\sim$ 5% damage level and analysed by the channeling-backscattering technique were compared with the previous results of Thompson and Walker[14]. In all cases the disorder level agreed within experimental accuracy. However, samples prepared for TEM have a disorder level below the detection limit of the channeling technique, and thus could be compared with the above results solely through a linear extrapolation.

Figure 9 illustrates the previous results of the disorder/ion (N_D^*) for irradiation of silicon at 35 K as a function of the energy deposited in nuclear collisions. The empirical results are contrasted with the model of Kinchin and Pease, and it should be noted that the deviation from the linear approximation increases with ion mass. An empirical expression was developed relating N_D^* to $\nu(E)$ and the projectile mass. By assuming the collisional and spike components of the disorder separable, and the spike component to be in the form of a spherical amorphous zone,

spike diameters (Figure 10) were derived. The insensitivity of spike diameter to ion energy is immediately evident, in contrast to WSS theory. A similar trend was observed in TEM observations - qualitatively an artifact of the R^3 scaling of highly localized disorder (where R is the linear cascade dimension).

However, the extrapolation from channeling measurements to disordered zones should be regarded with considerable caution. The model assumes the disorder in excess of that predicted by Kinchin and Pease to be in the form of a spherical amorphous zone. As pointed out previously, the channeling technique gives solely an indication of the gross features of lattice disorder - not at all of microscopic structure. Predictions of microscopic details based on channeling measurements can only be based on crude physical models such as the "energy spike".

5.2.2 Previous TEM Measurements of Ion Bombarded Solids

Several accounts of observation of small, highly disordered regions in metals and covalently bonded solids by TEM have appeared in the literature. Mazey et al.[18] have reported on 80 KeV Ne bombardment of silicon at room temperature and elevated temperatures. The lowest fluence $\sim 10^{13}/cm^2$ produced disordered zones $\sim$ 5 nm in diameter, until further irradiation $\gtrsim 10^{14}/cm^2$ led to overlap and finally to an amorphous surface layer.

Norris[19] has observed vacancy clusters in metals at depths comparable to the ranges of the bombarding ions for 80-150 KeV heavy ion bombardment. Studies of heavy ion damage in α iron[20] has shown a strong connection between the energy density (and hence cascade compactness) and the development of damage structures in irradiated metals.

Low temperature irradiations (< 30 K) of germanium by 100 KeV O^- ions[21] led to formation of disordered regions ∿ 9 nm in diameter which were concluded to be amorphous. Typically one region was observed for each five ions, in contrast with the results of the present study for lower energy heavy ions on silicon, where the correspondence was observed to be much closer to 1:1. Room temperature irradiations by O^- led to regions of smaller average diameter (∿ 7 nm). One advantage of this study was that irradiations and analysis could be performed in-situ whereas measurements in the present study were on samples which had annealed for over long periods at room temperature. Nevertheless, Parsons was limited to a single species, whereas this work has allowed the extension of TEM investigations to high energy density regimes at fluences where cascade overlap is negligible.

5.2.3 Comparison of Cascade Distributions with "Energy Spike" Predictions and WSS

Figures 4(a)-(f) illustrate the size distribution for heavy ion cascades in silicon for six ion species. As pointed out previously, all monatomic cascades except 15 KeV Bi "tail" toward the larger diameters. One possible contribution although only for 15 KeV As ($1.05 \times 10^{12}/cm^2$) is an overlap contribution leading to larger zones not indicative of a single cascade. Due to the limitation of measuring samples annealed to room temperature the distribution observed may not be that which existed at 50 K; although general trends remain unaffected. Another possible contribution is an artifact of the size measurement, involving an average of the maximum and minimum linear dimensions of the disordered region. As evident from simple geometric considerations, the equivalent spherical

diameter is probably overestimated for those regions with a large difference in the two linear dimensions - where transverse straggling is more important. Hence this effect is expected to scale directly with energy and inversely with mass ratio. Thus the 15 KeV Bi distribution would be expected to exhibit the least asymmetry.

Similar considerations apply to the diatomic irradiations (60 KeV Bi_2, 40 KeV Sb_2). The 40 KeV Sb_2 distribution is broad; perhaps an artifact of the smaller mass ratio (projectile/target) and hence increased transverse straggling. Those diatomic cascades of significant overlap might result in a large disordered zone, whereas a significantly more dilute cascade may be observed as two closely spaced zones after the anneal to room temperature. The Bi_2 bombardment, with the much increased mass ratio, exhibits much less transverse straggling. Experimentally the distribution is approximately Gaussian.

The criteria established for analysis of electron micrographs take no account of subcascade structure but rather assume each distinct contrast region to represent an individual cascade. This is probably the most reasonable assumption for comparison of disorder levels, in that the contrast region is assumed to represent an approximate boundary between highly disordered crystal and a perfect lattice. Some uncertainty in the correlation between channeling measurements and TEM resides with the uncertainty of the relation between the microscopic features of disorder and the backscattering yield. Nor is it known what fraction of the disorder which anneals between 50 K and room temperature would be observed with TEM. Herein lies an important assumption - that the disordered zones observed with TEM at room temperature can reasonably be related to the magnitude of the disorder detected by channeling at 35 K. As

previously mentioned, the annealing effects are known to be large, so that it is impossible to make a truly direct comparison except by in-situ measurement.

In spite of experimental limitations, TEM observations strongly support the highly non-linear heavy ion induced disorder indicated in earlier studies with the channeling technique. This can be clearly seen by a comparison with transverse straggling predicted by WSS theory.

The WSS transverse cascade dimension increases with decreasing ion mass, qualitatively a result of the increased mean free path. Observed differences between WSS cascade dimensions and the TEM results indicate that only a small portion of the WSS volume is amorphous, this fraction depending on the nature of the implanted ion.

Similar conclusions are reached by extrapolation from channeling measurements based on the "energy spike" model. The "channeling diameters" of Figure 10 indicate the same trend as the TEM observations. As pointed out by J. Westmoreland and P. Sigmund[22] an $E^{2/3}$ scaling of the cluster diameter would be predicted by the WSS theory for these scattering regimes. Contrary to the inverse scaling of cascade volume with mass ratio (WSS), both TEM and channeling measurements predict an increasing disordered volume with projectile mass. From Table I, average diameters for 15 and 60 KeV Bi cascades are respectively 4.3 nm and 5.0nm; whereas WSS theory predicts 4.0 nm and 10.5 nm, $\sim E^{2/3}$ scaling. Cascade diameters (from WSS, TEM and channeling) are summarized in Table IV, from which it is evident that TEM and channeling predict a similar energy and mass scaling.

The comparison of the parameter dependence of cascade size is

more significant than the comparison of the absolute magnitudes of cascade diameters. In general, the largest discrepencies for cascade diameters between TEM or channeling and the WSS theory are expected for the lower ion mass irradiations, since the cascade disorder is relatively dilute. Initial investigations of 100 keV P^+ irradiation, revealing very small disordered regions for high fluence ($7.5\times10^{12}/cm^2$) provides an extreme example. WSS would predict a diameter of 54 nm. This is a regime where neither channeling nor TEM samples disordered regions associated with a single ion.

To facilitate comparison with channeling results, a relative disorder parameter, D^*, a function of the cascade diameter and observed number density is defined:

$$D^* = \sum_i \left(f_i \times \text{number density} \times 10^{-11} \right) \times \left(\text{average diameter} / 10 \right)^3$$

where the summation is over all size intervals of the cascade distribution, and f_i is the fraction of the area under the distribution curve in segment "i". The D^* parameter will prove to be a useful quantity for comparison of annealing results where relative changes for a single specimen are evaluated. The D^* function, however, is not employed to compare different irradiations due to its several limitations.

A major uncertainty and an inherent insensitivity of TEM is the R^3 scaling of cascade size - a small change in R leading to a large change in volume. In addition, contrast regions of equal dimension may not have the same structure nor exert the same influence on the surrounding lattice. Furthermore, the sensitivity of the channeling technique to relaxation effects poses a limitation on the comparison of measurements. In light of the various limitations, detailed quantitative comparisons will not be attempted here; qualitative comparisons will be made to investigate the

validity of various physical models.

Although the comparison of room temperature cascade volumes with the low temperature channeling results is subject to uncertainty from annealing effects, the higher temperature annealing correlation eliminates this limitation.

5.2.4 Comparison of TEM and Backscattering Analysis of Annealing Behaviour

Radiation induced defects react to reduce the free energy of a solid. In simplest form, the annealing rate is proportional to an exponential factor, exp[-E/KT], where E is the "activation energy". In reality, analysis is complicated, even for relatively simple defect structures, since annealing processes often overlap, precluding observation of a unique activation energy. Thus, unfolding of the activation energies for the highly disordered regions produced by heavy ion bombardment has not been attempted.

Calculations of relative damage (D*) have been performed for anneal stages investigated by TEM, with the results summarized in Table V. Figure 11 shows the TEM points (with estimated uncertainty), superimposed on the channeling curves. Note that in two cases the energy comparisons are not exact (40 KeV Sb_2 vs 30 KeV Sb_2 and 20 KeV As vs 15 KeV As) but the general trends are not expected to be affected. If anything 30 KeV Sb_2 points would shift toward the channeling curve because of increased energy density. The correlation between the channeling-backscattering results and the TEM predictions is very good. In general a consistency with annealing between 50 K and room temperature as detected by the channeling technique is observed - As, Bi, Sb_2 in increasing order of thermal stability, as was pointed out in section 4.2 .

The annealing of radiation disordered silicon is critically dependent on the defect concentration and distribution. The highest anneal temperatures are observed for the two dimensional regrowth of amorphous surface layers, where several TEM studies[18],[23],[24] indicate recovery at $\sim 600^{\circ}C$. The TEM studies of Mazey[18], discussed in section 5.2.2, indicated that the observed 5 nm non-crystalline zones were stable up to $400^{\circ}C$ - $500^{\circ}C$. Since the disordered zones were produced by 80 keV Ne irradiation at 300 K, cascade overlap effects are significant, leading to a significantly different lattice structure between amorphous regions - as opposed to isolated "spikes" of the heavier ions. J.W. Mayer et al.[25] concluded from channeling investigations of the annealing of room temperature implantation of silicon that two extreme annealing regimes exist: recovery at $\sim 600°C$ for the amorphous surface layers and recovery at 200°C - 300°C for the isolated cascades. However, the present study indicates that the lower fluences still had a non-neglibigle contribution from cascade overlap. Significant annealing, for example, occurs between 100°C and 150°C for all monatomic bombardments in this work. The good correlation between TEM and channeling investigations do indicate, however, that the fluences used for the latter represent a good approximation to negligible cascade interaction, since fluences for TEM were typically an order of magnitude lower.

Table VI lists average energy densities of cascades in silicon determined from equation (5) of section 5.1.3. The average maximum energy density refers to the complete overlap of atomic cascades. The work by Thompson and Walker outlined earlier indicated that the disorder (indicated by the channeling-backscattering technique) created by

heavy ion irradiation of silicon could not be described as a unique function of energy density. In fact those authors chose to use the nuclear energy loss as the independent parameter in an empirical expression which also incorporates the mass ratio.

Nor does the thermal stability of the disorder bear a unique monatonic relation to the average energy density. This is evident by comparison of the average energy densities for 15 KeV Bi and 30 KeV Sb_2: 1.20 eV/atom and 0.79 eV/atom respectively. Whereas the Bi induced disorder shows definite annealing at 100°C, the diatomic antimony are stable to 150°C.

Over wide ranges of energy density, however, a general scaling is expected. In fact, the thermal stability of the monatomic and diatomic irradiations show this behaviour individually: 15 KeV Bi (1.20 eV/atom) → 15 KeV Sb (0.59 eV/atom) → 15 KeV As (0.31 eV/atom) and 30 KeV Bi_2 (1.76 eV/atom) → 30 KeV Sb_2 (0.79 eV/atom).

Annealing characteristics may also be related to the cascade size observed with TEM. In this case the scaling shows: 40 KeV Sb_2 (4.6 nm and 5.1* nm) → 15 KeV Bi (4.3 nm) → 20 KeV Sb (3.9 nm) → 20 KeV As (3.0 nm). A distinct trend is apparent but there are limitations to comparison:

(1) The distribution shape is not accounted for in the simple average. The 40 KeV Sb_2 sample is a particular case and point.

(2) Energy effects with associated straggling may change observed cascade size without a comparable change in amorphous volume - that is, the observed size is not indicative of a perfect amorphous "spike" volume.

(3) There is an inherent insensitivity of the TEM measurements through the R^3 scaling of the disordered volume.

(4) The various assumptions may not affect different measurements to the

---

* investigation 7 months after the first

same degree, hence leading to a distortion of relative comparisons.

Thus TEM does not offer a means of unfolding the subtle differences between the cascade structure. However, in good agreement with channeling measurements, it reveals general and consistent trends in the irradiation and annealing behaviour of heavy ion damage in silicon.

5.3 Implications for Basic Physical Processes

5.3.1 Limitations of Experimental Technique

Before outlining the major conclusions of this correlation study, the experimental limitations are summarized.

TEM measurements are subject to uncertainty in length measurement and the physical interpretation of strain contrast. In addition to the subjective nature of measurements, the reference temperature is not well defined, since sample preparation involves cleaning in boiling benzene (80°C). Fortunately, as evident from annealing results, this is only a serious consideration for the 20 keV As irradiation.

Sensitivity of the total disorder (R^3 scaling) to the linear cascade dimension has been pointed out previously. Also the TEM technique used here is relatively insensitive to energy effects in that the image is a projected one. An initial dilute track may anneal before a denser spike region but not be detected by projected contrast imaging.

Another uncertainty in the correlation of the two techniques is the difference in disorder necessary for reliable measurements. As pointed out in discussion of the annealing results, however, the 5% disorder levels used in channeling-backscattering studies seems a reasonable approximation to isolated cascade structure.

Thus, although TEM and channeling-backscattering provide different and complementary techniques for the investigation of radiation damage, various experimental uncertainties impose limitations on the interpretation of data. In addition to those points discussed above, the two probes have other inherent drawbacks. In the case of channeling - the He stopping power, energy and dosimetry lead to systematic errors in the absolute determination of disorder. Also the MeV ion beam itself has a disordering effect which cannot be neglected in the channeling annealing studies. In TEM this corresponds to e^- irradiation effects as well as heavier ion bombardment from sputter emission of the filament.

Finally, the samples used in this study were prepared at the Tandem Accelerator Laboratory at McMaster University and later analysed at Chalk River. Due to limitations of surface effects (long term oxidation) as well as the unexpected degree of room temperature annealing, it is suggested that as far as possible further correlation studies should be performed in-situ.

5.3.2 Summary

The results of this experimental study form perhaps three basic conclusions.

First the excellent correlation of the channeling-backscattering results and TEM measurements indicate that the techniques detect similar disorder in the lattice, at least at room temperature and above for heavy ion irradiation of silicon. This is particularly evident in the annealing results with the TEM data incorporated in a spherical amorphous volume model.

Secondly, as with the earlier channeling work, no unique scaling with energy density is apparent. To some extent one is limited by the insensitivity of TEM to the measurement of subtle differences of cascade structure. Size scaling of the zones offers some evidence of thermal stability, but once straggling and energy effects are taken into account, this criterion is found to be definitive only for large differences in cascade dimension. The positive result is that in comparison with channeling, no discrepency in the description of heavy ion irradiated silicon is evident.

Finally, the study has implications for the amorphization process. Previous estimations of the critical defect density to initiate the crystalline to amorphous transition have ranged from 2%[26] to 50%[27]. Caution must be exercised, however, in extrapolating predictions from equilibrium physics models for high energy density regimes. Also experimental results seem to indicate that there is no unique amorphous state - at least as determined by these probing techniques. Regions which differ little in size were found to exhibit very different annealing behaviour. This should be compared with the recent results of Beanland and Williams[28] where variations in the epitaxial regrowth rate for As^+/As_2^+ and Sb^+/Sb_2^+ implants in silicon were observed. This indicates that the nature of the disorder depends critically on the implanted ion. The study outlined in this present work demonstrated this for isolated cascades; Beanland and Williams showed that this was also the case for two dimensional regrowth of amorphous surface layers.

TABLE I

SIZE DISTRIBUTION DATA FOR ION-IRRADIATED SILICON

(IRRADIATION AT 50 K, OBSERVED AT 300 K)

Ion	Average Diameter (nm)	Average Number Density (cm^{-2})	Normalized Distribution Histogram							
			1 - 2 nm	2 - 3 nm	3 - 4 nm	4 - 5 nm	5 - 6 nm	6 - 7 nm	7 - 8 nm	8 - 9 nm
60 KeV Bi	5.0	2.95×10^{11}		0.28	0.75	1.0	0.84	0.57	0.29	0.06
60 KeV Bi_2	5.6	2.39×10^{11}		0.12	0.33	0.71	1.0	0.73	0.32	0.08
15 KeV Bi	4.3	2.11×10^{11}		0.25	0.82	1.0	0.41			
20 KeV Sb	3.9	2.61×10^{11}		0.42	1.0	0.68	0.26	0.06		
40 KeV Sb_2	4.6	2.65×10^{11}		0.5	1.0	0.95	0.82	0.77	0.29	0.07
40 KeV Sb_2*	5.1	2.59×10^{11}		0.41	0.61	0.85	1.0	0.97	0.55	
20 KeV As	3.0	6.04×10^{11}	0.28	1.0	0.51	0.31	0.09			

*sample examined after 7 months R.T. annealing from initial observation indicated directly above.

TABLE II

ANNEALING OF RADIATION DAMAGE IN SILICON BY THE CHANNELING BACKSCATTERING TECHNIQUE

30 KeV Sb_2 ($1.95 \times 10^{12}/cm^2$)		30 KeV Bi_2 ($1.2 \times 10^{12}/cm^2$)		15 KeV As ($1.0 \times 10^{13}/cm^2$)		15 KeV Sb ($4.5 \times 10^{12}/cm^2$)		15 KeV Bi ($3 \times 10^{12}/cm^2$)	
T_A	F_D	T_A	F_D	T_A	F_D	T_A	F_D	T_A	F_D
R.T.	1.0	R.T.	1.0	R.T.	1.0	R.T.	1.0	R.T.	1.0
98	1.03	138	1.02	80	0.66	87	0.80	96	0.97
138	0.99	167	0.95	101	0.62	120	0.69	136	0.85
170	0.99	190	1.04	120	0.48	140	0.58	165	0.75
190	0.84	225	1.00	140	0.43	161	0.53	188	0.64
215	0.73	250	0.82	160	0.29	180	0.30	212	0.50
250	0.70	293	0.53	179	0.27	200	0.23	230	0.37
290	0.45	330	0.34	200	0.23			260	0.26
320	0.23	350	0.19	220	0.13				
340	0.13								

T_A indicates anneal temperature (10 minute anneals) in degrees Celsius

F_D indicates the fractional remaining damage

TABLE III

TEM INVESTIGATION OF THE ANNEALING OF ION-IRRADIATED SILICON

Ion	T_A	Average Number Density (cm^{-2})	Normalized Distribution Histrogram						
			1 - 2 nm	2 - 3 nm	3 - 4 nm	4 - 5 nm	5 - 6 nm	6 - 7 nm	7 - 8 nm
40 KeV Sb_2 (3×10^{11})	R.T.	2.59×10^{11}		0.41	0.61	0.85	1.0	0.97	0.55
	160	2.37×10^{11}		0.41	0.72	0.69	0.80	1.0	0.47
	245	1.81×10^{11}		0.40	0.74	1.0	0.88	0.63	0.26
	297	1.49×10^{11}		0.26	0.88	1.0	0.61	0.28	0.06
	327	1.10×10^{11}		0.35	0.77	1.0	0.81	0.35	0.05
15 KeV Bi (3×10^{11})	R.T.	2.11×10^{11}		0.25	0.82	1.0	0.41		
	145	1.88×10^{11}		0.27	0.78	1.0	0.44		
	200	1.63×10^{11}		0.47	0.99	1.0	0.28		
	255	0.50×10^{11}	0.51	0.81	1.0	0.38	0.03		
20 KeV As (1.05×10^{12})	R.T.	6.04×10^{11}	0.28	1.0	0.51	0.31	0.09		
	145	2.85×10^{11}	0.48	0.83	1.0	0.50	0.04		
	200	0.80×10^{11}	0.14	1.0	0.86	0.38			

T_A indicates anneal temperature in degrees Celsius (10 minutes anneals)
Initial ion fluence indicated in brackets (50 K irradiation)

TABLE IV

PREDICTED CASCADE DIAMETERS BY TEM, WSS*, AND CHANNELING**

Incident Ion	TEM Diameter (nm)	WSS Diameter (nm)	Channeling Diameter (nm)
15 keV Bi	4.3	4.0	5.5
60 keV Bi	5.0	10.5	7.3
60 keV Bi_2	5.6	6.4	>8.2†
20 keV As	3.0	8.7	4.6
40 keV Sb_2	4.6 , 5.1††	7.8	7.3
20 keV Sb	3.9	7.8	5.2

* $\langle y^2 \rangle^{1/2} \times 2$, i.e. twice the mean transverse straggling

** from Figure 10 and reference (14)

† The value indicated is for twice the disorder induced by a 30 keV Bi irradiation; the enhancement due to cascade overlap has not been measured.

†† The sample was examined after 7 months of room temperature annealing from the initial observation of 4.6 .

TABLE V

FRACTIONAL REMAINING DAMAGE BY TEM ASSUMING A SPHERICAL CASCADE VOLUME

20 KeV As (1.05 x $19^{12}/cm^2$)		15 KeV Bi (3 x $19^{11}/cm^2$)		40 KeV Bi_2 (2 x $10^{11}/cm^2$)	
T_A	F_D	T_A	F_D	T_A	F_D
R.T.	1.0	R.T.	1.0	R.T.	0.90
145	0.49	145	0.91	1.65	0.90
200	0.13	200	0.65	245	0.56
		255	0.12	297	0.35
				327	0.28

T_A is the anneal temperature in degrees Celsius

F_D is the fractional remaining damage

*original irradiations at 50 K; fluence indicated in brackets

TABLE VI

AVERAGE ENERGY DENSITIES FOR HEAVY

ION CASCADES IN SILICON

Ion	Volume Ratio for Monatomic Cascade	Average Energy Density (eV/atom)	Average Maximum Energy Density for Diatomic Cascade (eV/atom)
15 keV Bi	0.63	1.20	–
30 keV Bi_2	0.63	1.76	2.40
60 keV Bi	0.63	0.13	–
20 keV Sb	0.50	0.42	–
40 keV Sb_2	0.50	0.56	0.84
15 keV Sb	0.50	0.59	–
30 keV Sb_2	0.50	0.79	1.18
15 keV As	0.47	0.31	–

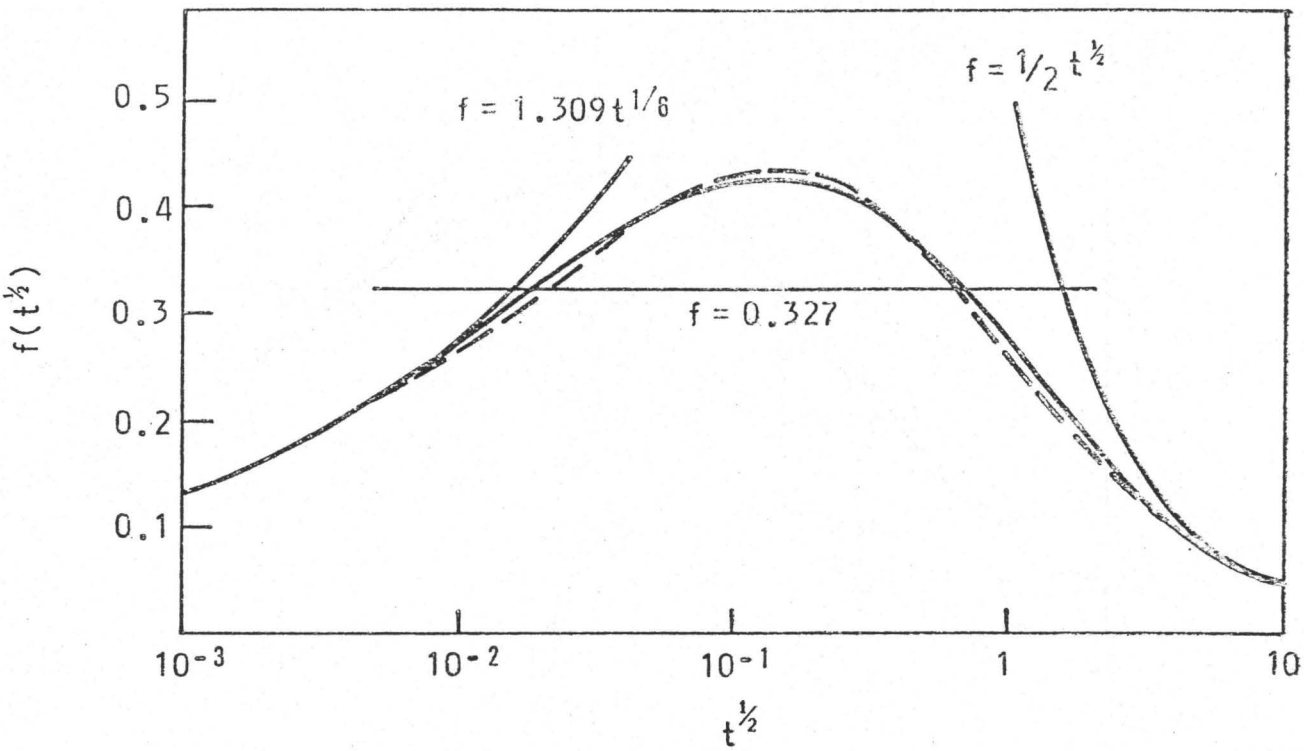

Figure 1(a): The Universal Screening Function

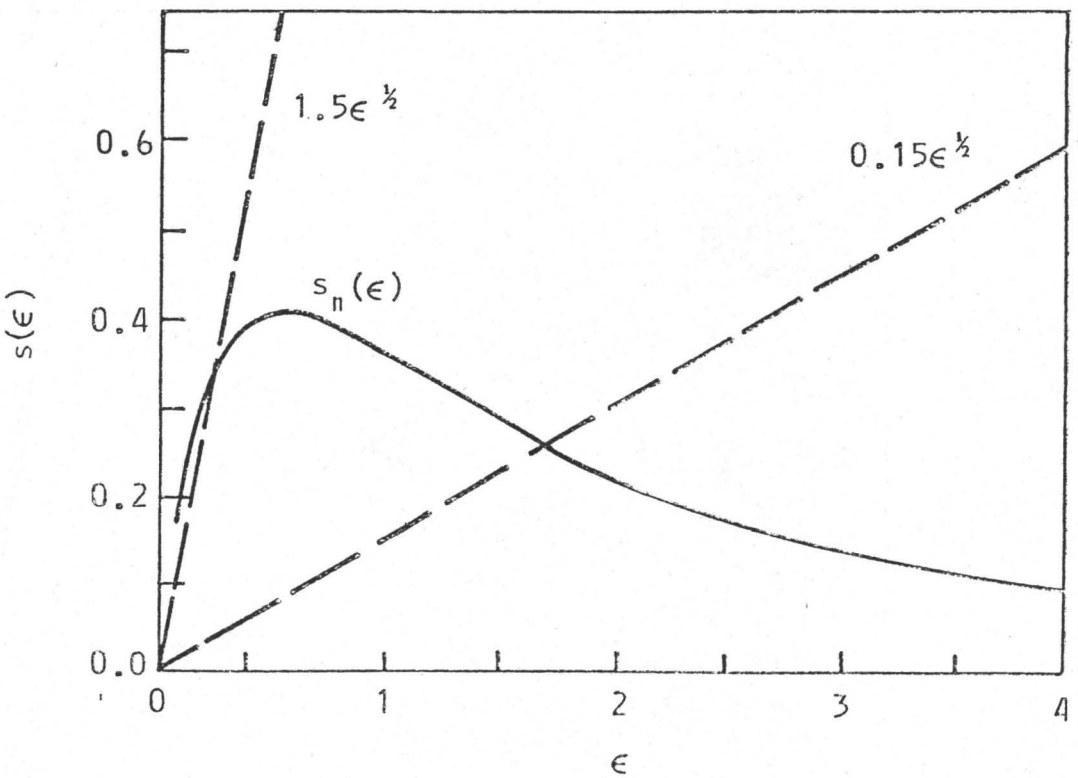

Figure 1(b): The Universal Nuclear Stopping Cross Section

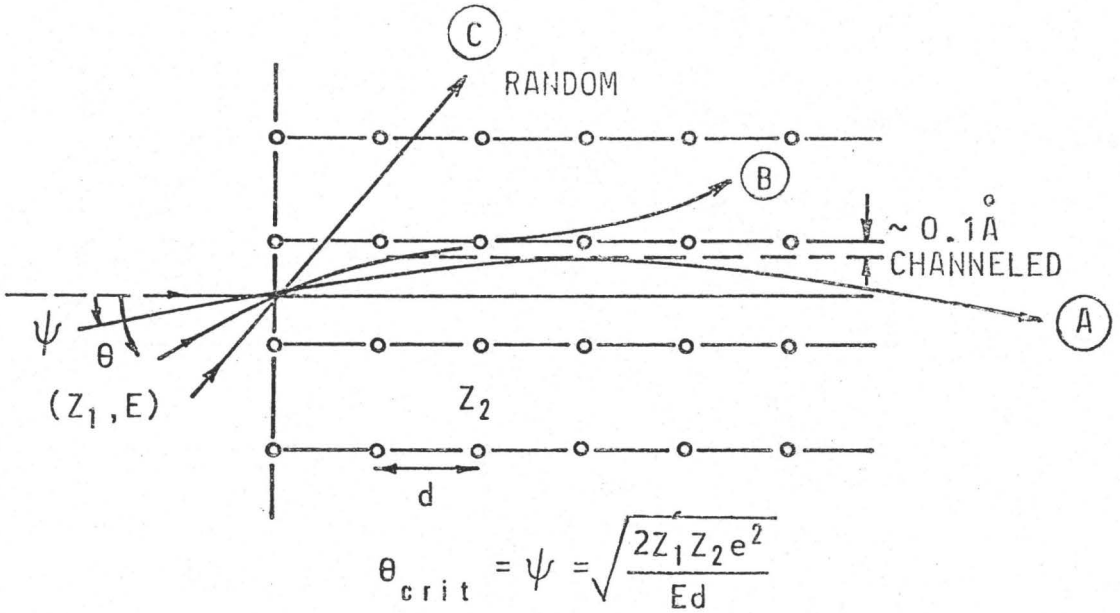

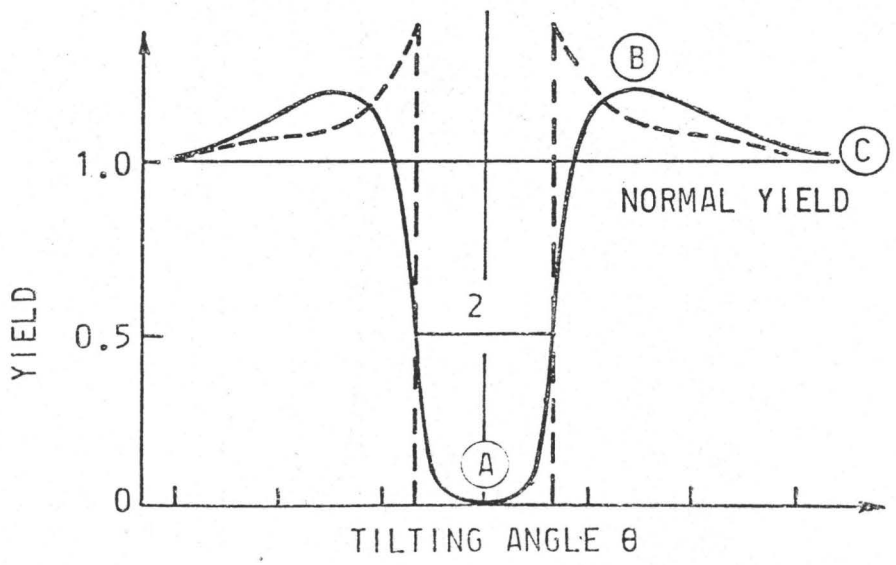

Figure 2: Illustration of the Channeling Phenomenon

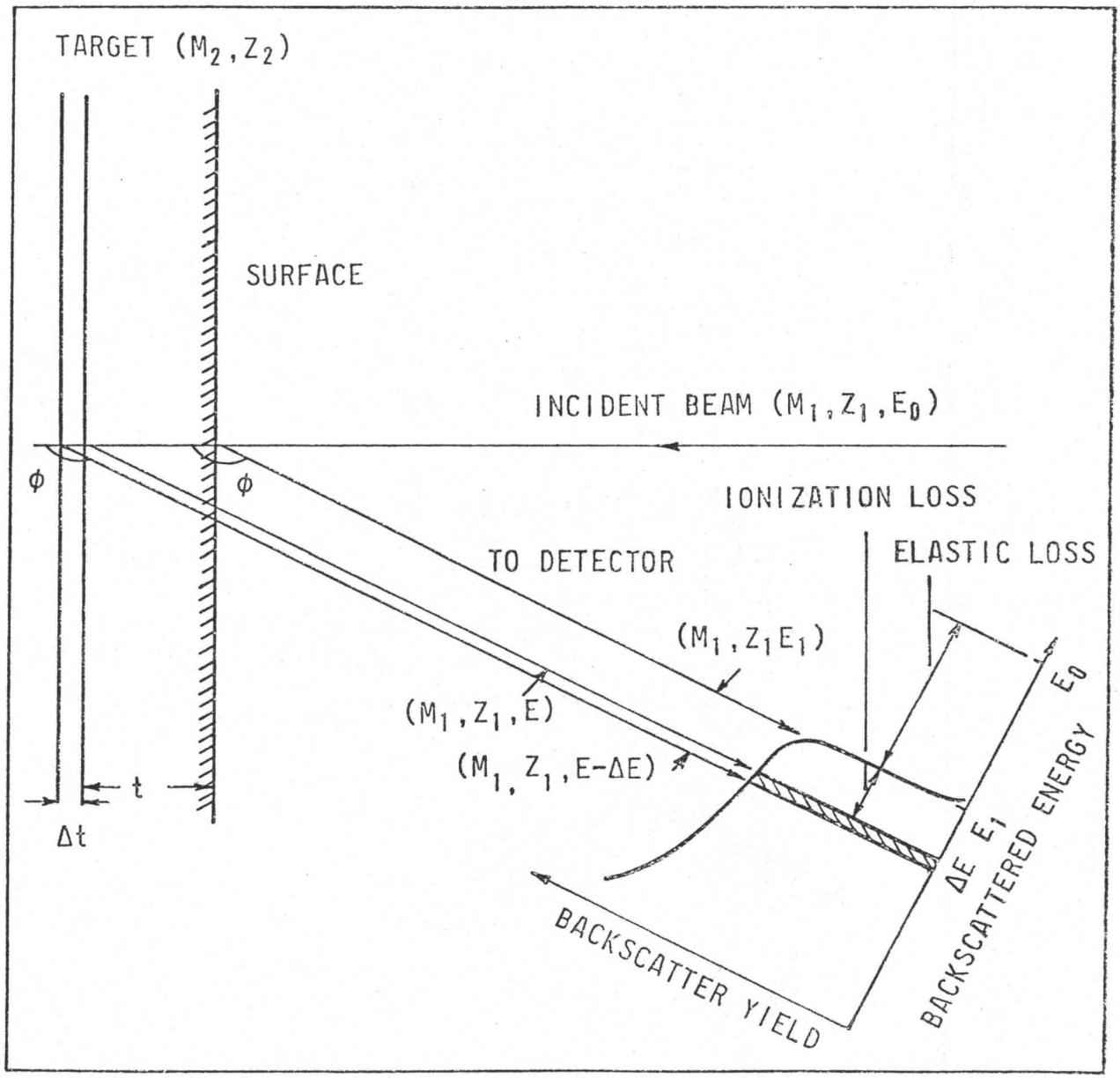

Figure 3: Principles of Backscattering Spectrometry

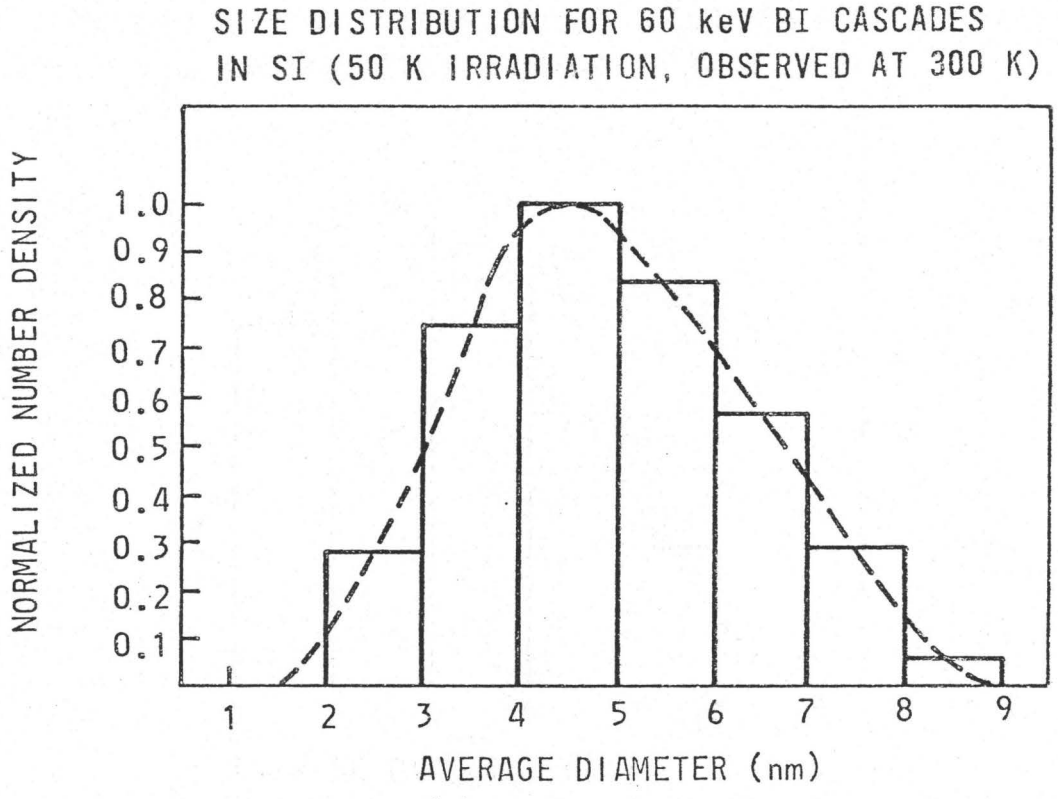

Figure 4(a): 60 keV Bi Distribution

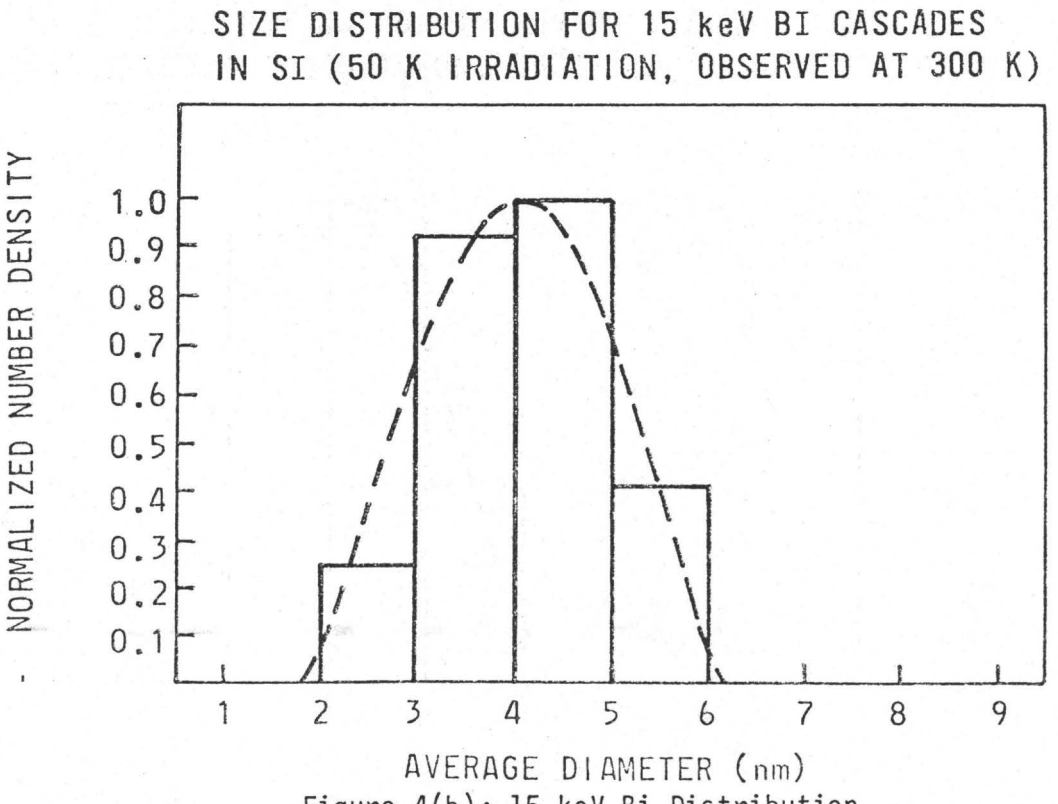

Figure 4(b): 15 keV Bi Distribution

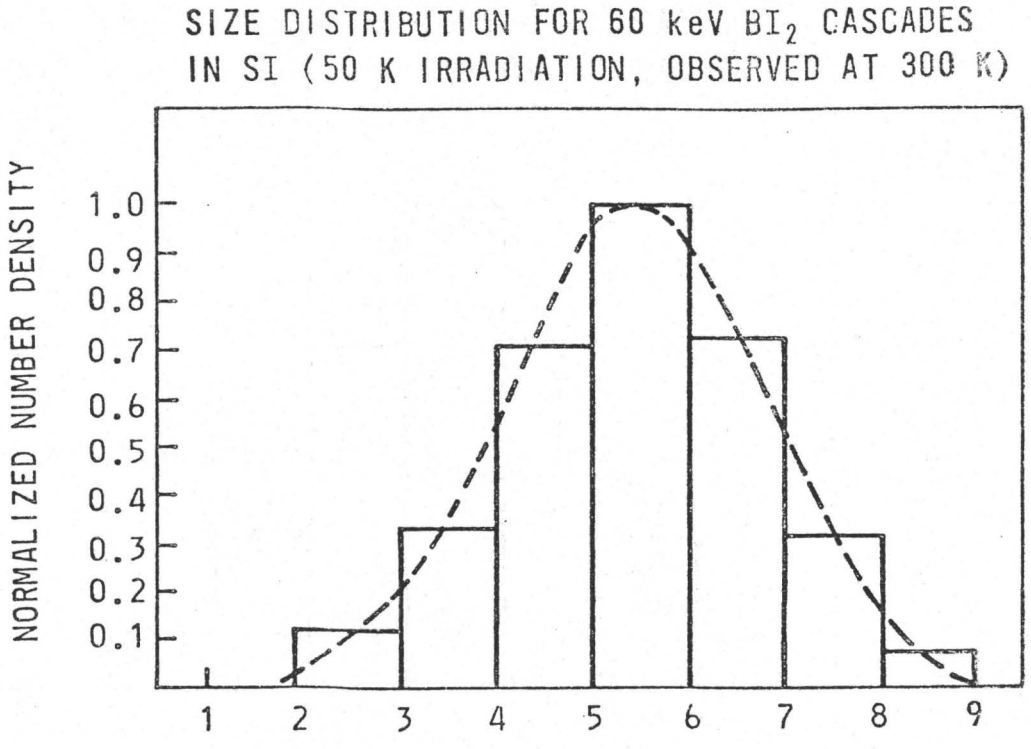

Figure 4(c): 60 keV Diatomic Bi Distribution

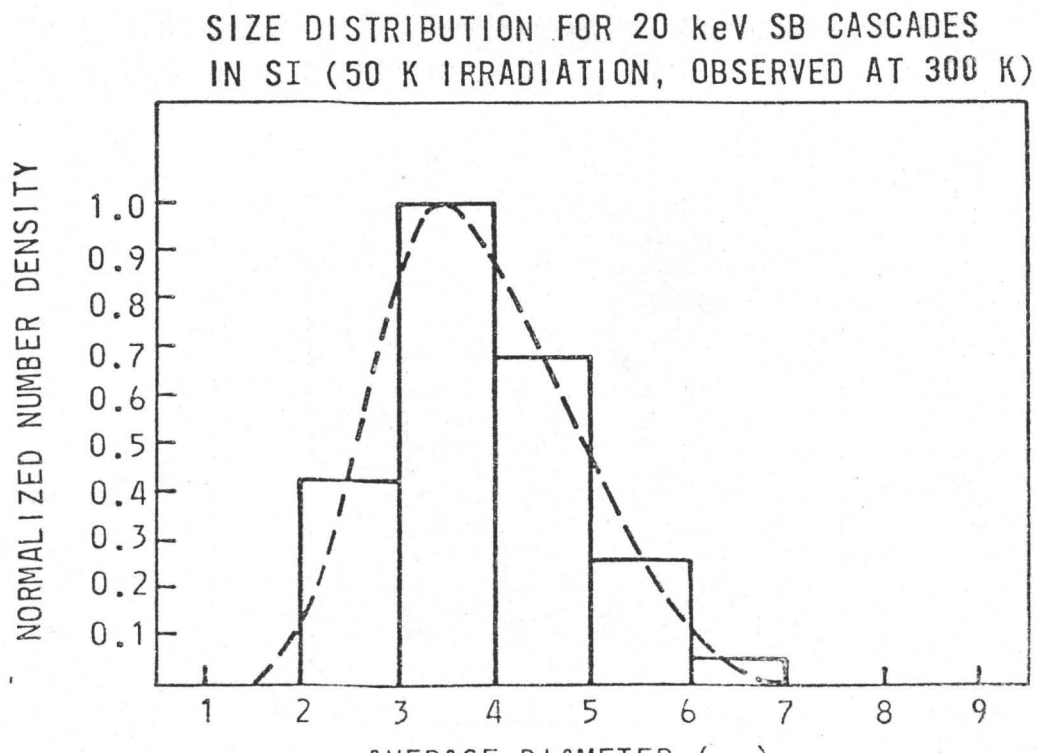

Figure 4(d): 20 keV Sb Distribution

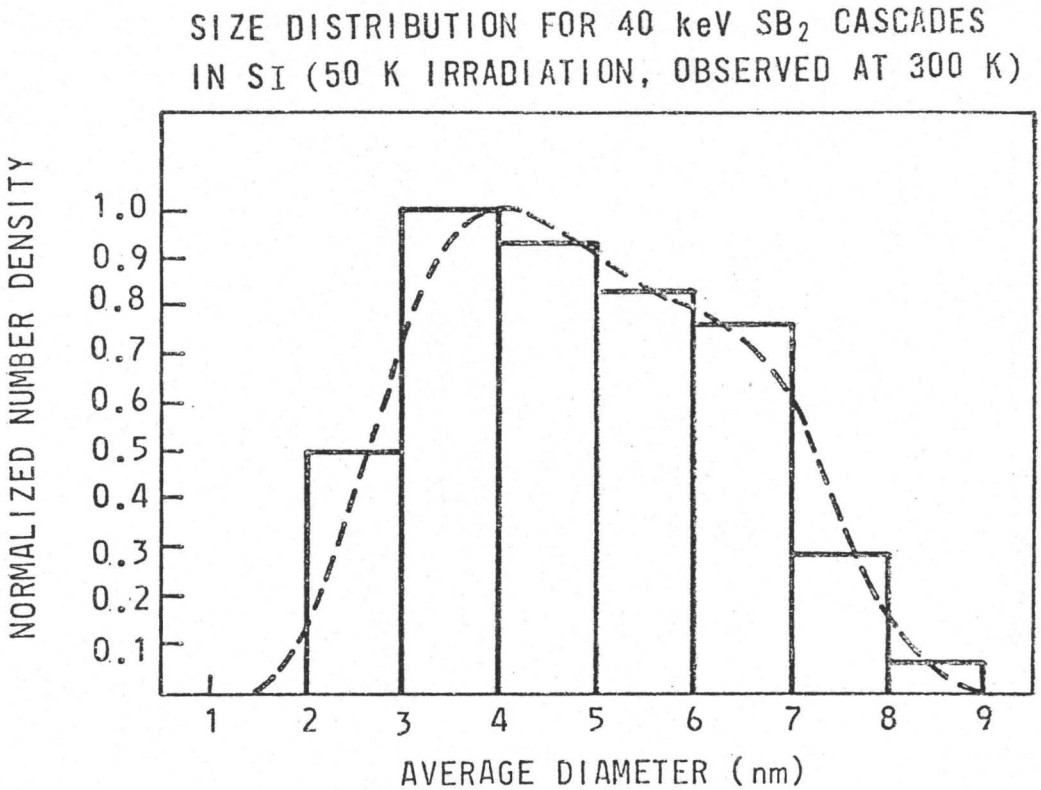

Figure 4(e): 40 keV Diatomic Sb Distribution

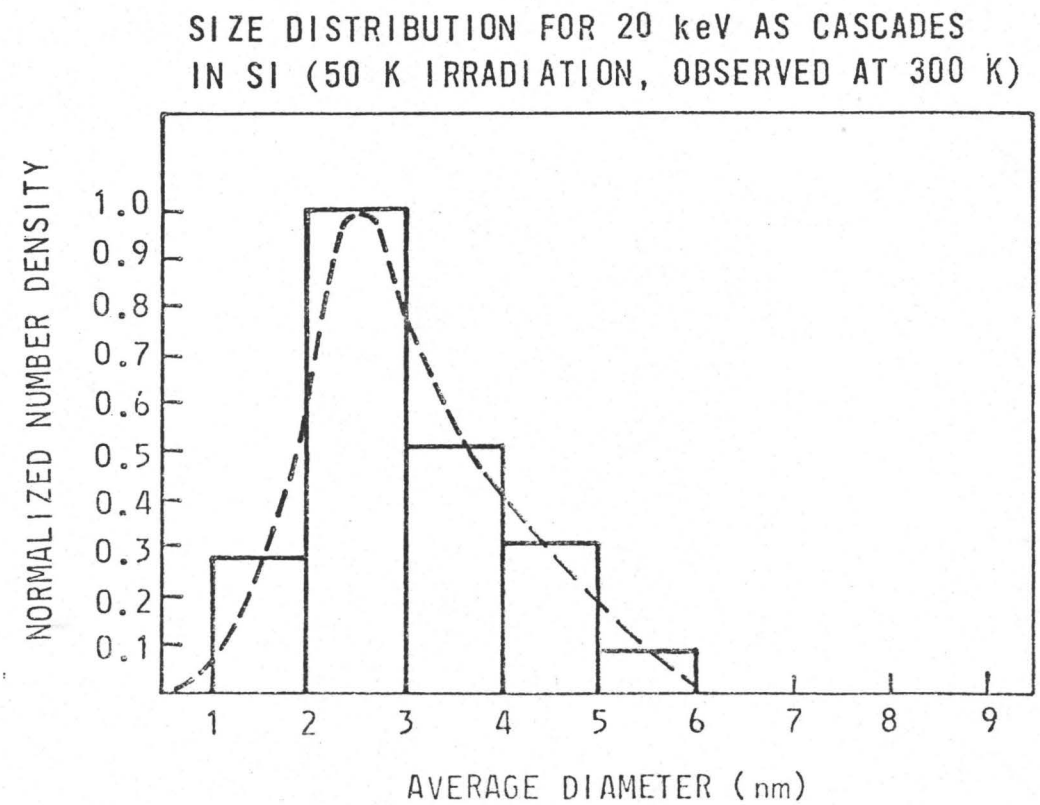

Figure 4(f): 20 keV As Distribution

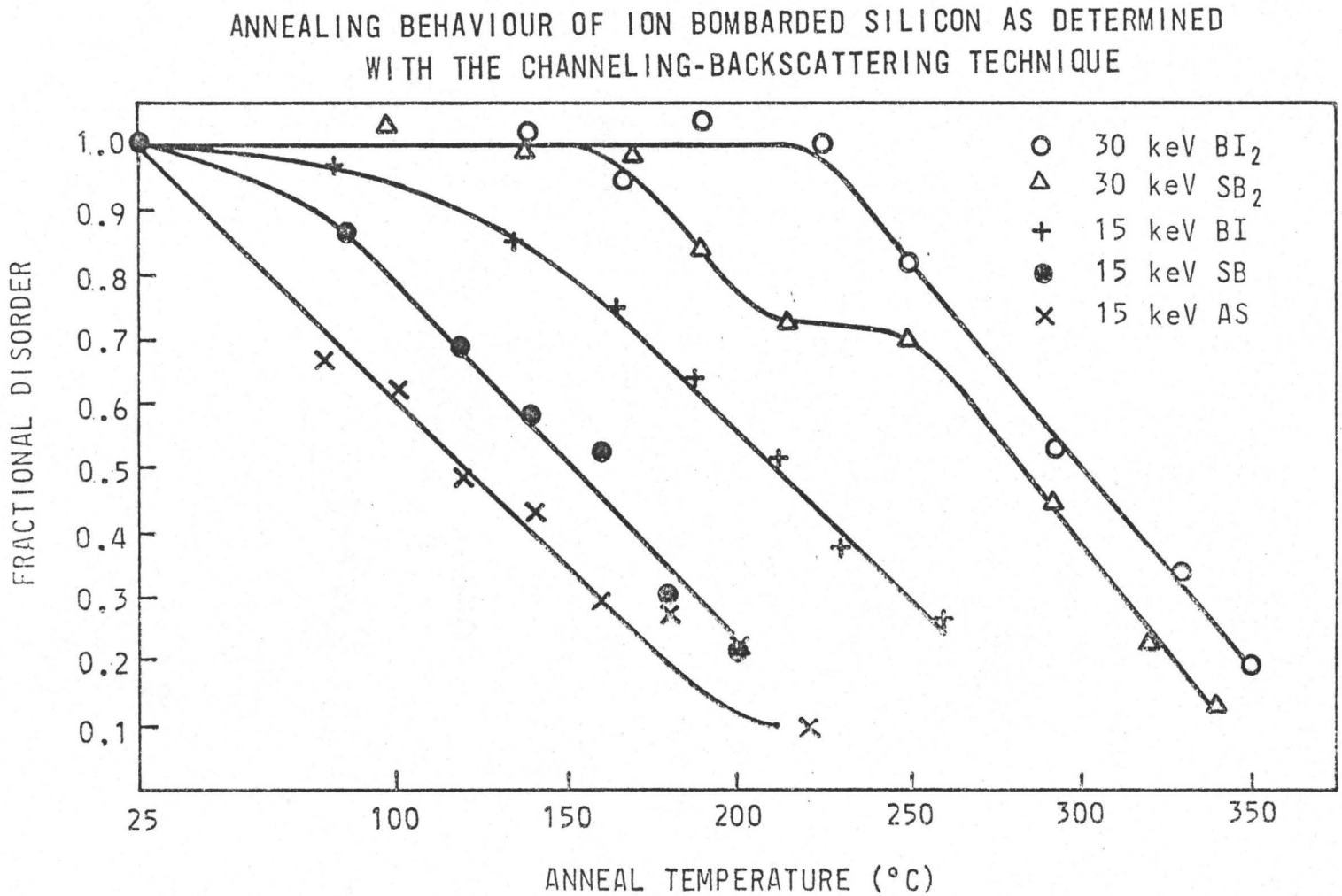

Figure 5: Annealing Behaviour - Channeling Study

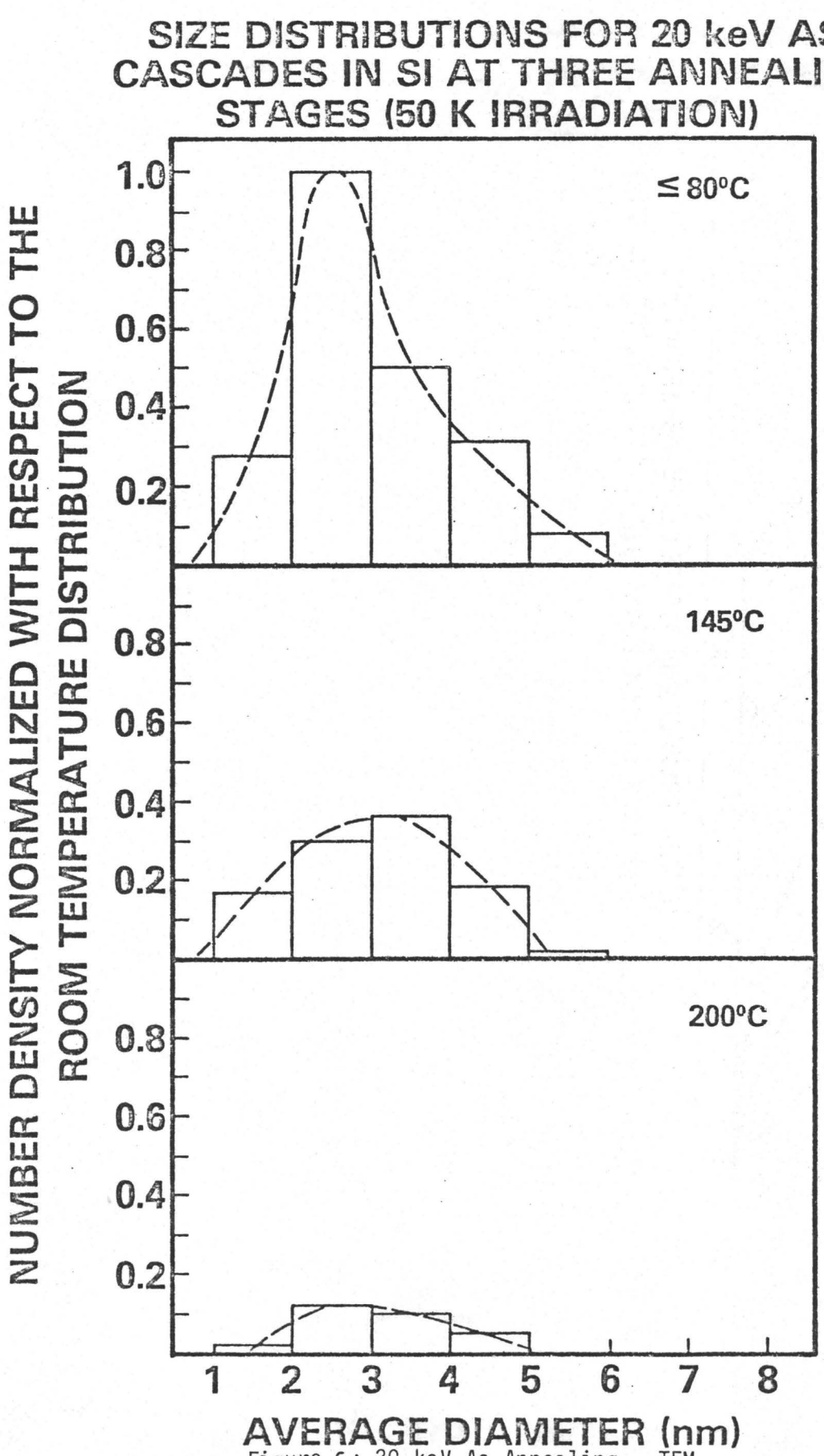

Figure 6 : 20 keV As Annealing - TEM

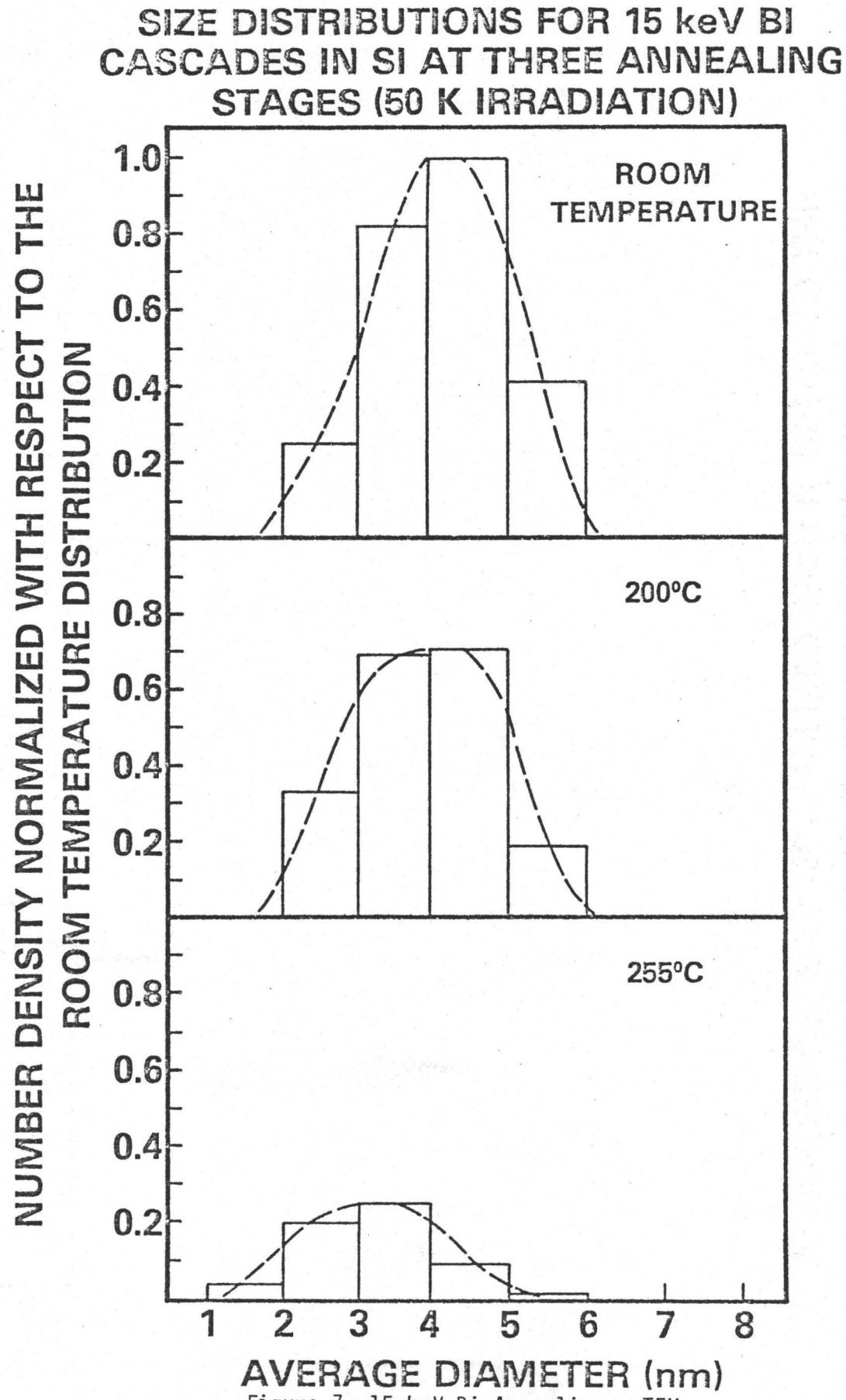

Figure 7: 15 keV Bi Annealing - TEM

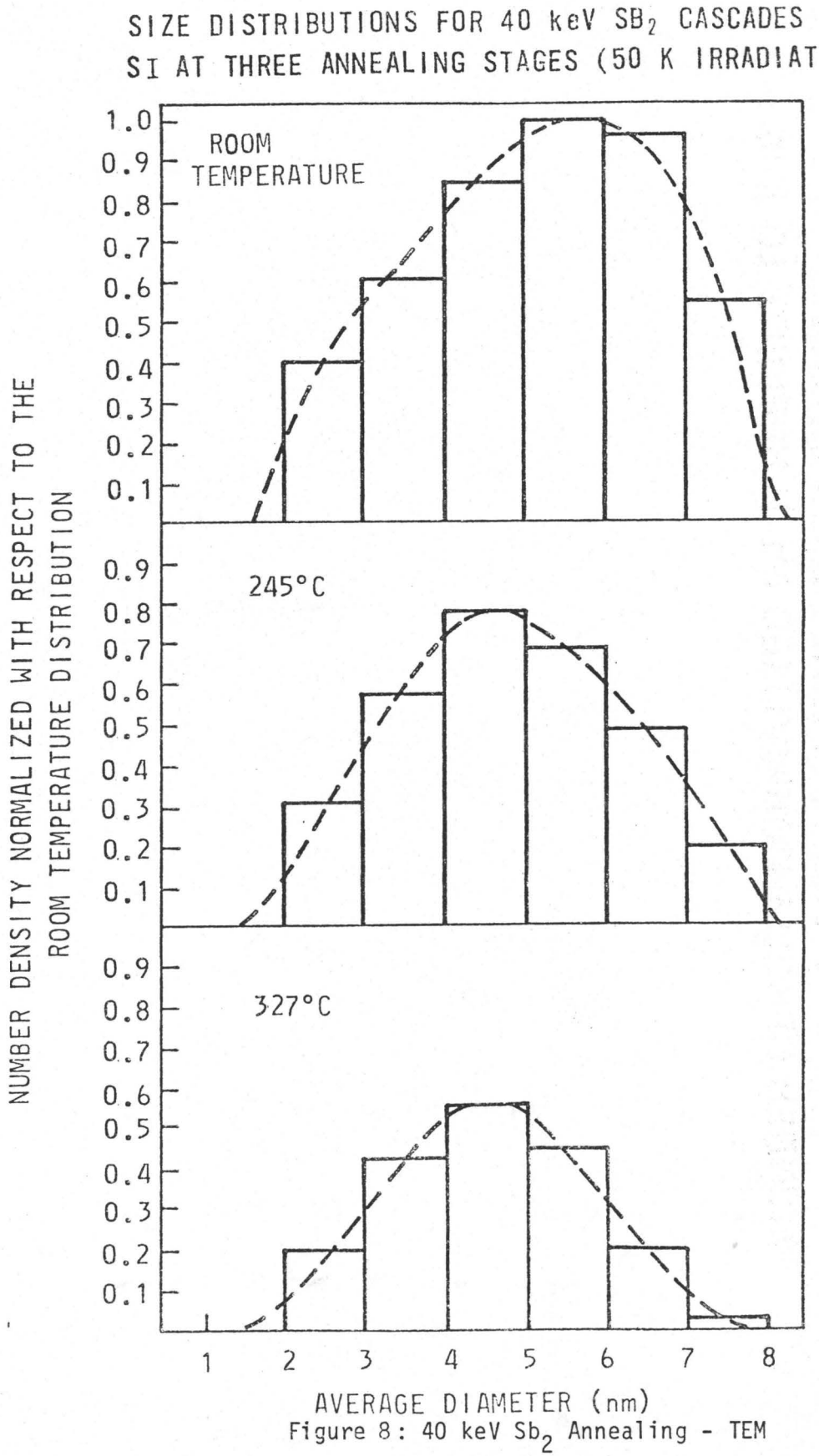

Figure 8: 40 keV Sb_2 Annealing - TEM

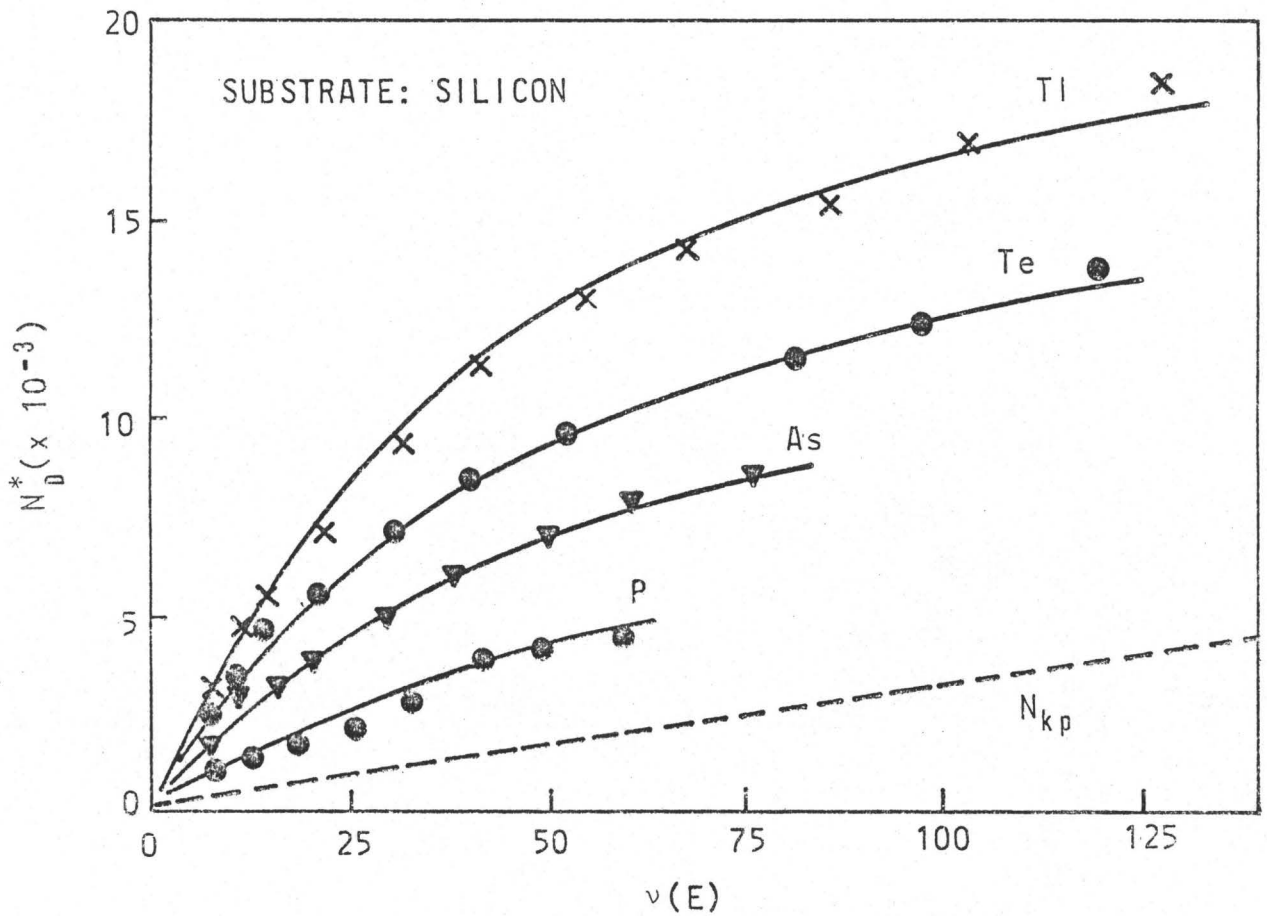

Figure 9: N_D^* (Displacements/Ion) vs. Nuclear Energy Loss

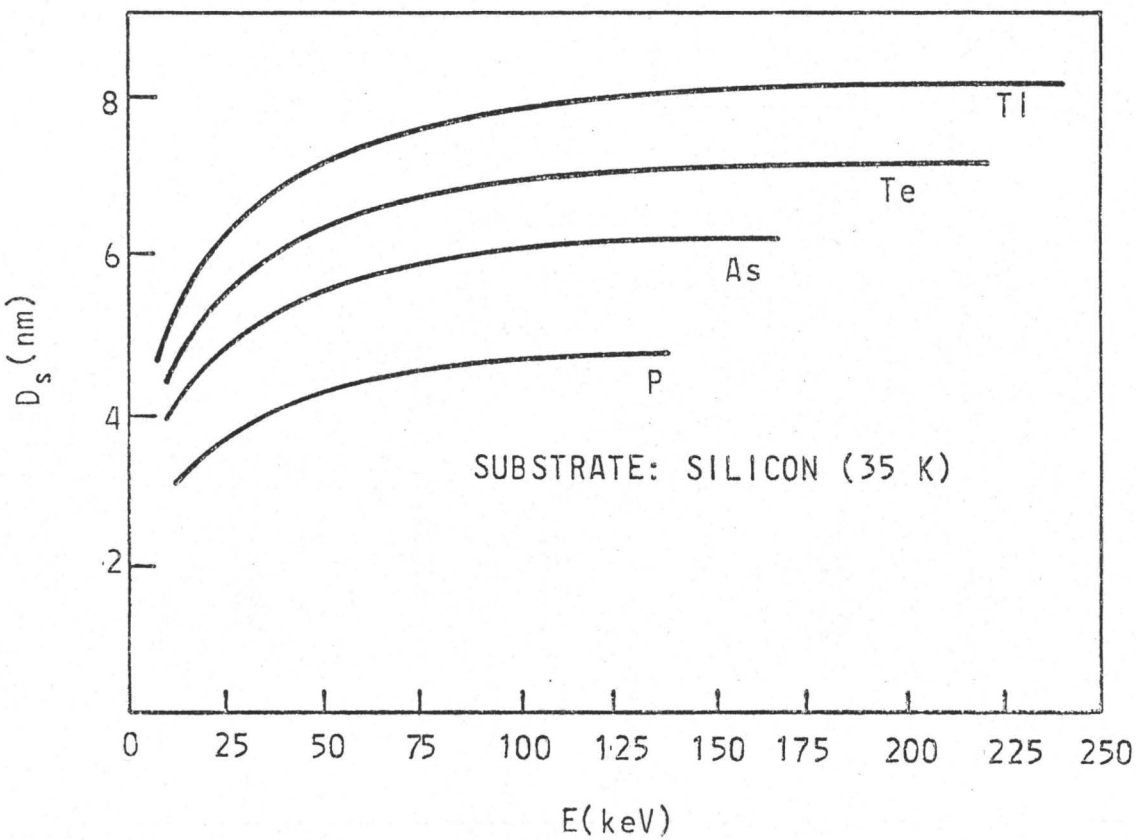

Figure 10: Equivalent Diameters Predicted from Channeling

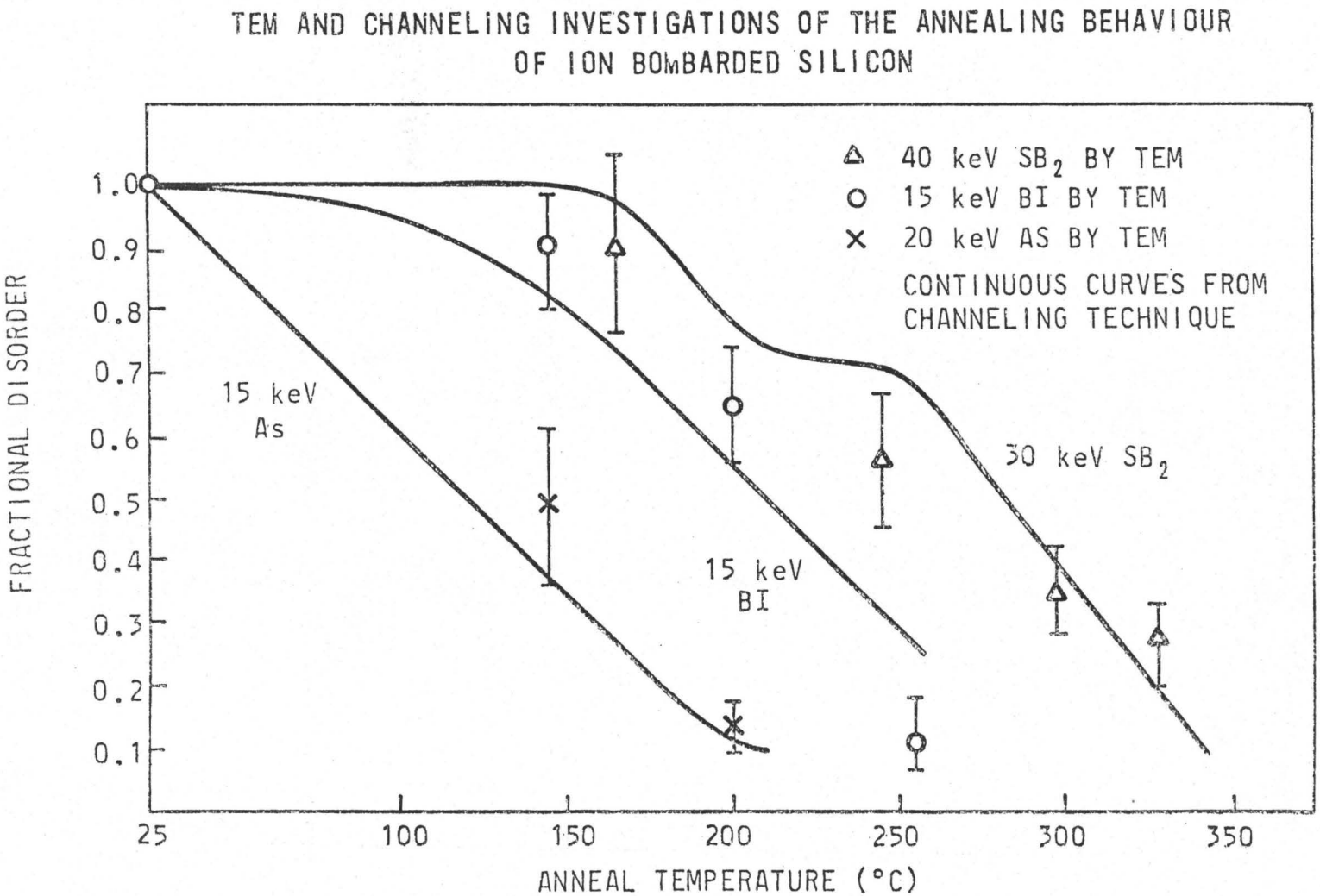

Figure 11: Correlation of TEM and Channeling in Annealing Studies

REFERENCES

(1) J. Lindhard et. al., Kgl. Dan. Vid. Selsk. Mat. Fys. Medd. 33 , no. 10 (1963)

(2) O.B. Firsov, Engl. Transl. Sov. Phys. JETP 9, 1076 (1959)

(3) H.A. Bethe, Intermediate Quantum Mechanics. Benjamin, New York, Amsterdam, Ch. 15

(4) U. Fano, Ann. Rev. Nucl. Sci. 13, 1. (1963)

(5) M. Inokuti, Rev. Mod. Phys., 43, 297. (1971)

(6) J. Lindhard et. al., Kgl. Dan. Vid. Selsk. Mat. Fys. Medd. 36, no. 10 (1968)

(7) M.W. Thompson, Defects and Radiation Damage in Metals, Cambridge University Press, London, 1969.

(8) S. Namba, Ion Implantation in Semiconductors, Plenum, p.385 (1975)

(9) D.S. Gemmel, Rev. Modern Phys. 46, 129 (1974)

(10) D.V. Morgan, Channeling - Theory, Observation and Applications, J. Wiley and Sons, London.(1973)

(11) D.A. Thompson and R.S. Walker, Radiation Effects, 30, 37. (1976)

(12) B. Beeston et. al., Electron Diffraction and Optical Diffraction Techniques, North Holland. (1973)

(13) U. Valdre, Electron Microscopy in Materials Science, Acedemic Press, New York, London. (1971)

(14) D.A. Thompson and R.S. Walker, Radiation Effects, Vol. 36, p. 91 . (1978)

(15) P. Sigmund, Appl. Phys. Letts., 25, no. 3, 169. (1974)

(16) Roger Kelly, Radiation Effects, 32, 91. (1977)

(17) J.A. Davies, et. al., Phys. Rev. Letts., Vol. 34, No. 23, 1441. (1975)

(18) D.J. Mazey, R.S. Nelson and R.S. Barnes, Phil. Mag. 17, 1145. (1968)

(19) D.I.R. Norris, Proc. Int. Conf. Atomic Collision Phenomena in Solids, North-Holland, p. 97. (1970)

(20) C.A. English, B.L. Eyre, M.L. Jenkins, Nature, Vol. 263, 400. (1976)

(21) K.J.R. Parsons, Phil. Mag. 12, 1159. (1965)

(22) J.E. Westmoreland and P. Sigmund, Radiation Effects, 6, 187. (1970)

(23) S. Namba, Ion Implantation in Semiconductors, Plenum, p. 21. (1975)

(24) S. Namba, Ion Implantation in Semiconductors, Plenum, p. 473. (1975)

(25) J.W. Mayer et. al., Can. J. Phys., 46, 663. (1968)

(26) M.L. Swanson, J.R. Parsons and C.W. Hoekle, Radiation Effects, 9, 249. (1971)

(27) F.L. Vook and H.J. Stein, Radiation Effects, 2, 23. (1969)

(28) D.G. Beanland and J.S. Williams, Radiation Effects, 36, 15. (1978)